Measurement Report: Elevated excess-NH₃ can promote the redox reaction to produce HONO: Insights from the COVID-19 pandemic

Xinyuan Zhang[1,2], Lingling Wang[3], Nan Wang[3], Shuangliang Ma[3], Shenbo Wang[2,4] *, Ruiqin Zhang[2,4]**, Dong Zhang[1,2], Mingkai Wang[2,4], Hongyu Zhang[1,2].

[1]College of Chemistry, Zhengzhou University, Zhengzhou, 450000, China

[2]Research Institute of Environmental Sciences, Zhengzhou University, Zhengzhou 450000, China

[3]Henan Provincial Ecological Environment Monitoring and Safety Center, Zhengzhou, 450000, China

[4]School of Ecology and Environment, Zhengzhou University, Zhengzhou, 450000, China

Correspondence: Shenbo Wang (shbwang@zzu.edu.cn) and Ruiqin Zhang (rqzhang@zzu.edu.cn)

Abstract

The incongruity between atmospheric oxidizing capacity and NO_x emissions during the COVID-19 pandemic remains puzzling. Here, we show evidence from field observations of ten sites in China that there was a noticeable increase in NH_3 concentrations during the COVID-19 pandemic. In addition to the meteorological conditions, the significant decrease in sulfate and nitrate concentrations enhanced the portioning of NH_4^+ to NH_3. Such conditions enable enhanced particle pH values, which in turn accelerate the redox reactions between NO_2 and SO_2 to form HONO. This mechanism partly explains the enhanced atmospheric oxidizing capacity during the pandemic and highlights the importance of coordinating the control of SO_2, NO_x, and NH_3 emissions.

1. Introduction

Atmospheric oxidizing capacity (AOC) is an important parameter that affects the formation of secondary aerosols and O_3 (Li et al., 2021a; Wang et al., 2023b). Identifying the factors influencing AOC is crucial for further reducing particulate matter and O_3 pollution. During the COVID-19 pandemic, unprecedented control measures were implemented, resulting in significant reductions in emissions from mobile traffic and stationary industry sources (Zheng et al., 2020; Wang et al., 2020a; Tian, 2020). However, studies have shown a surprising increase in AOC during this period (Huang et al., 2021a; Li et al., 2023; Liu et al., 2021; Wang et al., 2021; Zheng et al., 2020). Multiple studies have indicated that the sharp decrease in nitrogen oxide (NO_x) emissions leads to a substantial increase in O_3, as well as daytime OH and HO_2 radicals, and nighttime NO_3 radicals, subsequently resulting in an overall increase in AOC (Huang et al., 2021a; Li et al., 2023; Liu et al., 2021; Zheng et al., 2020). However, the exact relationship between NO_x and AOC remains unclear.

Nitrous acid (HONO) is a critical precursor of OH radicals, contributing to more than 43–50% of OH production (Alicke, 2003) and exerting a strong influence on AOC(Zhang, 2023). Various sources of atmospheric HONO have been identified, including combustion processes (e.g., vehicle emissions) (Kramer et al., 2020; Liao et al., 2021a; Li et al., 2021b), direct emissions from soil (Su and Zhang, 2011; Oswald et al., 2013; Meusel et al., 2018), homogeneous reactions between NO and OH radicals (Pagsberg, 1997; Atkinson and Rossi, 2004), heterogeneous reactions of NO_2 on aerosols and ground surfaces (Zhang et al., 2020a; McFall et al., 2018; Liu et al., 2014; Liu et al., 2020a), and photolysis of nitrate (Spataro and Ianniello, 2014; Scharko et al., 2014; Romer et al., 2018; Ye et al., 2017; Shi et al., 2021). During the pandemic control periods, there was a substantial reduction in vehicle traffic flow and industrial emissions, leading to a decrease of more than 60% in NO_x emissions in eastern China(Huang et al., 2021a). It was initially expected that the concentration of HONO would also decrease proportionally. However, Liu et al. observed that the decrease in HONO

54   concentration during the pandemic period was only 31%, which was lower than the reductions

55   in NO (62%) and NO_2 (36%) (Liu et al., 2020b). Furthermore, it is worth noting that the

56   concentration of HONO during the COVID-19 pandemic in 2020 was higher compared to the

57   levels observed during the corresponding period in 2021 (Luo et al., 2023). This finding

58   suggests the existence of a considerable unknown source of HONO during the COVID-19

59   pandemic period.

60   Ammonia (NH_3) is a significant alkaline gas in the atmosphere that plays a crucial role in

61   the atmospheric nitrogen cycle (Gu et al., 2022; Xu et al., 2020; Gong et al., 2011). Several

62   studies have indicated that NH_3 can promote the formation of HONO by promoting the

63   hydrolysis of NO_2 (Xu et al., 2019) or the redox reaction of NO_2 with SO_2 (Liu et al., 2023).

64   Moreover, previous research has shown that NH_3 concentrations in the atmosphere,

65   particularly in rural areas, significantly increased during the pandemic (Xu et al., 2022).

66   Consequently, the rise in NH_3 may contribute to the enhanced formation of HONO and

67   subsequently enhance AOC. Unfortunately, there is currently a lack of research on the

68   relationship between enhanced NH_3 and AOC during the COVID-19 pandemic period.

69   To address this, online observational data on particulate matter composition, gaseous

70   pollutants, and meteorological conditions from ten sites in China before and during the

71   COVID-19 pandemic period were analyzed to investigate the variation in NH_3 concentrations

72   and particle pH and explore the promoting effect of increased pH values on HONO formation.

73   To the best of our knowledge, this is the first study to discuss the reasons for the increase in

74   AOC during the pandemic from the perspective of the influence of NH_3 on HONO.

75

2. Materials and methods

2.1 Observation sites

78   Online measurements were conducted at four urban and six rural sites from January 1 to

79   February 29, 2020, including Sanmenxia (U-SMX), Zhoukou (U-ZK), Zhumadian (U-ZMD),

80   and Xinyang (U-XY), as well as rural locations including Anyang (R-AY), Xinxiang (R-XX),

81   Jiaozuo (R-JZ), Shangqiu (R-SQ), Nanyang (R-NY), and Puyang (R-PY). Descriptions and

82   the spatial distribution of these ten sites can be found in Table S1 and Figure S1 of

83   Supplementary Material.

84   **2.2 Measurements**

85   The aerosol and gas monitor (MARGA, Metrohm, Switzerland) was used to analyze the

86   hourly water-soluble ions (Na^+, NH_4^+, K^+, Mg^{2+}, Ca^{2+}, Cl^-, NO_3^-, and SO_4^{2-}) in $PM_{2.5}$, as well as

87   gaseous species (NH_3, HNO_3, HCl, and $HONO$) at ten sampling sites. The MARGA

88   instrument is widely used (Chen et al., 2017; Stieger et al., 2019; Twigg et al., 2022). A

89   detailed description of the instrument and QA/QC can be found in Text S1. In brief, the

90   atmospheric sample passes through a $PM_{2.5}$ cut-off head, and both particles and gases enter a

91   wet rotating dissolution device for diffusion. Subsequently, the particles in the sample

92   undergo hygroscopic growth and condensation in an aerosol supersaturated vapor generator,

93   followed by collection and ion chromatographic analysis. The gases in the sample are

94   oxidized by H_2O_2 in the dissolution device, absorbed into a liquid solvent, and then entered

95   the gas sample collection chamber for ion chromatographic quantification. The range of

96   minimum detection limits for water-soluble ions was between 0.002 μg/m^3 (Cl^-) to 0.081

97   μg/m^3 (NH_4^+). Previous works have shown that HONO observations measured using this

98   system agree well with other observational services, a detailed description of HONO and its

99   uncertainty can be found in Text S3. Overall, the limit of detection for HONO was 4 pptv and

100   the uncertainty was estimated to be ±20%. In addition, Uncertainties of 20% are assumed for

101   the detection of NH_3 and NH_4^+, while uncertainties of 10% are assumed for other

102   components(Wang et al., 2020b; Wang et al., 2022).

103   The data for NO_2 and SO_2 were obtained from a series of instruments provided by

104   Thermo Fisher Scientific (USA). The hourly concentrations of organic carbon (OC) in $PM_{2.5}$

105   were analyzed using a carbon analyzer (Model 4, Sunset Laboratory., USA). A detailed

106   description of the NO_2, SO_2, and carbon analyzer can be found in Text S2. The smart weather

107   stations (LUFFTWS500, Sutron, Germany) were utilized for synchronized observation of

108   meteorological parameters including temperature and relative humidity (RH).

109   **2.3 Data analysis.**

110   **2.3.1 pH prediction.**

111   The thermodynamic model ISORROPIA-II was used to estimate the pH value of the

112   particles (Fountoukis, 2007) by inputting RH, temperature, K^+, Ca^{2+}, Mg^{2+}, total ammonia

113   ($TNH_x = NH_4^+ + NH_3$), total sulfuric acid (TH_2SO_4, SO_4^{2-}), total sodium (TNa, Na^+), total

114   chlorine (TCl, Cl^-), and total nitrate ($TNO_3 = NO_3^- + HNO_3$). The ISORROPIA model

115   calculated the particle hydrate ion concentration per volume of air (H_{air}^+) and particulate water

116   associated with inorganic matter (AWC_{inorg}). The aerosol pH value was calculated using the

117   following equation (Bougiatioti et al., 2016):

$$pH = -\log_{10}H_{aq}^+ = -\log_{10} \frac{1000H_{air}^+}{AWC_{inorg} + AWC_{org}} \qquad (2.1)$$

119   where the modeled concentrations for AWC_{inorg} and H_{air}^+ are $\mu g/m^3$, and AWC_{org} is the particle

120   water associated with the organic matters predicted using the following method:

$$AWC_{org} = \frac{m_s}{\rho_s} \frac{k_{org}}{\left(\frac{1}{RH} - 1\right)} \qquad (2.2)$$

122   where m_s is the mass concentrations of organic matter (OC×1.6), ρ_s is the organic density

123   (1.35 g cm^{-3}), and k_{org} is the organic hygroscopicity parameter (Liu et al., 2017; Wang et al.,

124   2023a). k_{org} is the organic hygroscopicity parameter and depends on organic functionality,

125   water solubility, molecular weight, and oxidation level. Han (Han et al., 2022) has reported

126   that the k_{org} generally increased with O: C ratios, with a range of $0 - 0.3$ for 23 organics,

127   including carboxylic acids, amino acids, sugars, and alcohols. Wang et.al(Wang et al., 2023a)

128   estimated that the uncertainties of k_{org} value (0.06) for pH only lead to $-1–3\%$ errors, which

129   can be neglected. Therefore, the value of 0.06 was selected in this paper. The model has two

130   calculation modes: the forward mode and reverse mode, and the aerosol dissolution systems

131 can be set to simulate a metastable state (aqueous phase) or stable state (aqueous and solid

132 phase). Studies have shown that the forward mode is less affected by instrument measurement

133 errors than the reverse mode (Ding et al., 2019; Song et al., 2018). Additionally, the minimum

134 average RH of about 55% was recorded during the sampling period at the ten sites. Thus,

135 ISORROPIA-II was run in the forward model for the aerosol system in the metastable

136 condition.

2.3.2 The HONO source analysis

138 The source rates of HONO include direct emission (P_{emi}), homogeneous reaction of NO

139 and •OH (P_{OH+NO}), heterogeneous reaction of NO_2 on the ground (P_{ground}) and aerosol ($P_{aerosol}$),

140 photo-enhanced heterogeneous reaction of NO_2 on the ground ($P_{ground+hv}$) and aerosol

141 ($P_{aerosol+hv}$), nitrate photolysis ($P_{nitrate}$), and unknown source ($P_{unknown}$). The detailed

142 methodology for its calculation is described in the Supplementary Material (**Text S4**)

2.3.3 Production rate of HONO through redox reaction of NO_2 with SO_2.

144 The redox reaction of NO_2 with SO_2 (R_1) is considered a crucial potential source of high

145 concentrations of HONO in Northern China (Cheng et al., 2019; Wang et al., 2016):

$$S(IV) + 2NO_2 + H_2O \rightarrow S(VI) + 2H^+ + 2NO_2^- \tag{R_1}$$
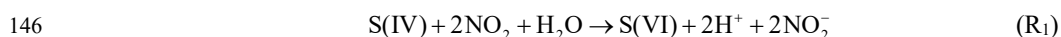
147 The rate expression for reaction (R_1) was estimated to:

$$d[S(VI)] / dt = k_1[NO_2][S(VI)], \tag{2.3}$$

149 The rate constant k_1 value is pH dependent, e.g., for pH, 5, $k_1 = (1.4\times10^5 + 1.24\times10^7)/2$ M^{-1}

150 s^{-1}. For k_1 values under other pH conditions and other related information, please refer to Text

151 S5, Table S2, and S3.

3. Results and discussion

152

3.1 Variations of NH_3, NH_4^+ and TNH_x.

153

154   The temporal variations of NH_3, NH_4^+, and TNH_x at 10 sampling sites in the pre-COVID-

155   19 pandemic period (PC, January 1 to 23, 2020) and during the COVID-19 pandemic period

156   (DC, January 24 to February 29, 2020) are presented in Figure 1, with their average

157   concentration listed in Table 1. In general, rural sites exhibited higher concentrations of NH_3,

158   NH_4^+, and TNH_x compared to urban sites, except for the R-NY site. This finding is consistent

159   with previous studies conducted in Zhengzhou (Wang et al., 2020b), Shanghai (Chang et al.,

160   2019), and Quzhou (Feng et al., 2022a), owing to the intense agricultural ammonia emissions.

161   The highest concentrations of NH_3 and TNH_x were recorded at site R-JZ, with average values

162   of 25.3 ± 11.5 and 40.8 ± 20.1 μg/m^3, respectively. Site R-AY had the highest NH_4^+

163   concentration, measuring 19.3 ± 12.9 μg/m^3. Note that the current study area exhibited higher

164   NH_3 levels compared to other regions (Table S4), which probably was attributed to the highest

165   NH_3 emissions of Henan Province in China, primarily from nitrogen fertilizer application and

166   livestock farming (Wang et al., 2018; Ma, 2020). Compared to the PC, NH_3 concentrations

167   increased in the DC at all sites. Notably, rural sites experienced more significant increases in

168   NH_3 concentrations than urban sites, which is similar to the trend in Shanghai (Xu et al.,

169   2022). The largest increases in NH_3 concentrations were observed at R-SQ (71%, 7.3 μg/m^3)

170   and U-ZK (37%, 4.8 μg/m^3) for rural and urban sites, respectively. In contrast, the

171   concentrations of NH_4^+ and TNH_x decreased in the DC with the largest reduction at rural site

172   R-PY (51%, 12.9 μg/m^3) and urban site U-ZMD (48%, 9.3 μg/m^3). Regarding TNH_x, rural

173   sites exhibited larger reductions, with site R-SQ experiencing the largest decrease of 37% (4.7

174   μg/m^3).
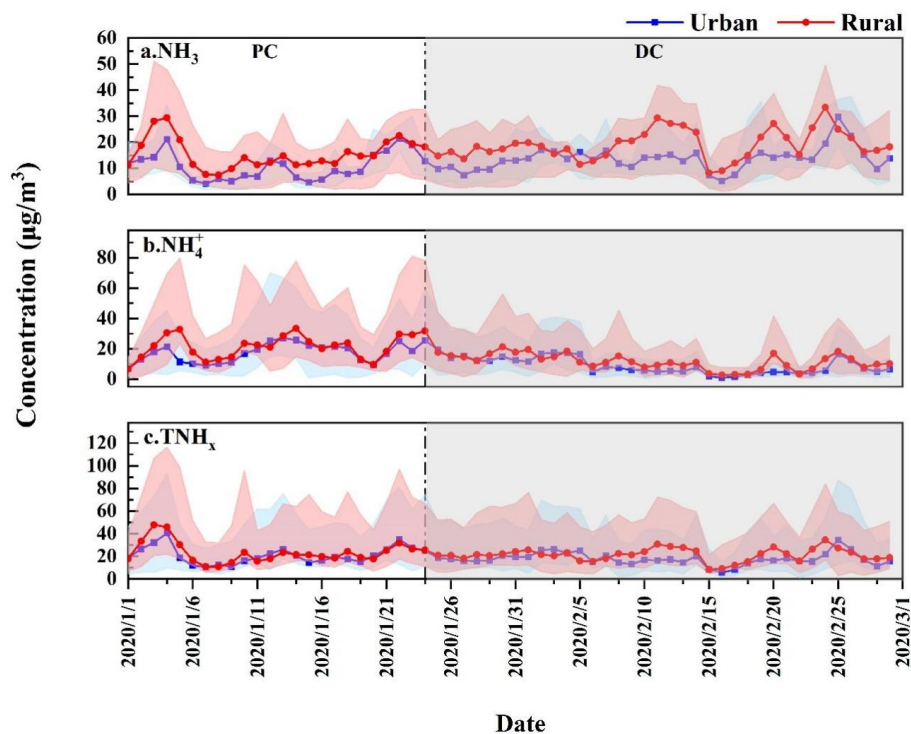
Figure 1. Temporal variations of a. NH_3, b. NH_4^+, and c. TNH_x at the urban and rural sites before (PC) and during (DC) the COVID-19 outbreak, respectively. The shaded areas of the curve represent the maximum and minimum values.

Table 1. Changes in concentrations (mean ± standard deviation) of NH_3, NH_4^+, and TNH_x at ten sites average (overall average for the period of observation), before (PC) and during (DC) the COVID-19 outbreak.

Site	Substance	Average (μg/m³)	PC (μg/m³)	DC (μg/m³)
U-SMX	NH_3	13.8 ± 10.8	12.6 ± 10.1	14.5 ± 11.1
	NH_4^+	10.9 ± 7.2	14.2 ± 7.2	8.8 ± 6.5
	TNH_x	22.9 ± 14.1	24.9 ± 14.5	21.7 ± 13.8
U-ZK	NH_3	15.6 ± 8.3	12.7 ± 6.5	17.4 ± 8.8
	NH_4^+	13.6 ± 9.3	19.1 ± 8.4	10.3 ± 8.1
	TNH_x	28.6 ± 13.7	30.9 ± 12.8	27.1 ± 14.0
U-ZMD	NH_3	13.1 ± 8.4	11.6 ± 8.2	14.0 ± 8.4
	NH_4^+	13.9 ± 9.8	19.6 ± 10.3	10.3 ± 7.5
	TNH_x	25.7 ± 14.6	30.3 ± 15.1	22.8 ± 13.5
U-XY	NH_3	7.0 ± 4.3	5.7 ± 4.0	7.9 ± 4.3
	NH_4^+	11.0 ± 7.7	15.4 ± 7.6	8.3 ± 6.5
	TNH_x	17.6 ± 9.8	20.6 ± 10.1	15.7 ± 9.2
R-AY	NH_3	19.0 ± 8.4	17.9 ± 8.3	19.7 ± 8.4
	NH_4^+	19.3 ± 12.9	26.4 ± 13.7	15.0 ± 10.3
	TNH_x	36.6 ± 18.2	41.7 ± 20.4	33.4 ± 16.0
R-XX	NH_3	21.7 ± 10.2	18.1 ± 9.3	23.8 ± 10.1
	NH_4^+	15.9 ± 10.4	20.6 ± 11.0	13.0 ± 8.8
	TNH_x	34.9 ± 17.0	35.1 ± 18.8	34.8 ± 15.8
R-PY	NH_3	19.8 ± 9.4	16.8 ± 8.1	21.7 ± 9.6
	NH_4^+	17.4 ± 11.8	25.3 ± 12.6	12.4 ± 8.0
	TNH_x	35.2 ± 17.8	39.4 ± 19.8	32.6 ± 15.7
R-JZ	NH_3	25.3 ± 11.5	24.1 ± 11.5	25.9 ± 11.4
	NH_4^+	17.3 ± 11.3	22.7 ± 11.6	14.2 ± 9.9
	TNH_x	40.8 ± 20.1	42.9 ± 22.8	33.5 ± 18.2
R-SQ	NH_3	15.0 ± 7.9	10.3 ± 5.2	17.7 ± 7.9
	NH_4^+	13.4 ± 8.5	18.9 ± 8.6	10.3 ± 6.7
	TNH_x	26.3 ± 13.2	25.5 ± 14.0	26.8 ± 12.7
R-NY	NH_3	5.5 ± 3.1	4.3 ± 2.7	6.2 ± 3.2
	NH_4^+	10.2 ± 6.9	13.3 ± 7.2	8.4 ± 6.1
	TNH_x	14.8 ± 8.5	16.0 ± 9.5	14.1 ± 7.8

Figure 2 illustrates the spatial distribution and the diurnal variation of NH_3 concentrations in the ten sites before and during the pandemic. NH_3 concentrations in most sites exhibited a unimodal trend in PC that NH_3 concentrations gradually increased after sunrise, reaching a peak around noon (11:00-12:00), and then decreased to a valley around 16:00-17:00. This diurnal pattern is similar to NH_3 variations observed in urban areas of Houston, USA, as a

189 result of the natural emissions from vegetation and soil during photosynthesis (Gong et al.,

190 2011). However, other studies have recorded a significant NH_3 peak during the early morning

191 of 8:00-10:00 (Ellis et al., 2011; Meng et al., 2018; Gu et al., 2022), suggesting the influence

192 of vehicle emissions (Gong et al., 2011; Gu et al., 2022), residual NH_3 mixing, soil or plant

193 emissions (Ellis et al., 2011), and dew volatilization (Wentworth et al., 2016; Huang et al.,

194 2021b). Therefore, the NH_3 in urban and rural areas of this study was less affected by NH_3

195 emissions from vehicles, different from the recent studies in megacities of China (e.g., Beijing

196 and Shanghai)(Gu et al., 2022; Wu et al., 2023; Zhang et al., 2020b). In addition to the

197 transport from agricultural emissions, urban NH_3 in this region may originate from other non-

198 agricultural sources, such as wastewater treatment, coal combustion, household waste, urban

199 green spaces, and human excrement (Chang et al., 2019).

200 During the COVID-19 pandemic, the diurnal variation of NH_3 in both urban and rural

201 sites still maintained a unimodal distribution. The peak values in urban sites remained

202 consistent with PC levels, further demonstrating that the influence of vehicles on NH_3 in

203 urban areas was limited. Notably, the peak time of NH_3 in rural sites shifted 1–2 hours earlier

204 compared to the trend in PC. Ammonia in rural areas primarily originates from nitrogen

205 fertilizer application, livestock, and poultry breeding (Feng et al., 2022a; Meng et al., 2018),

206 which are significantly influenced by temperature and RH (Liu et al., 2023). Table S5 and

207 Figure S2 reveal that the increased temperatures and decreased RH at rural sites in the PC,

208 could accelerate the evaporation of NH_3 and thus potentially lead to earlier peak NH_3

209 concentrations.
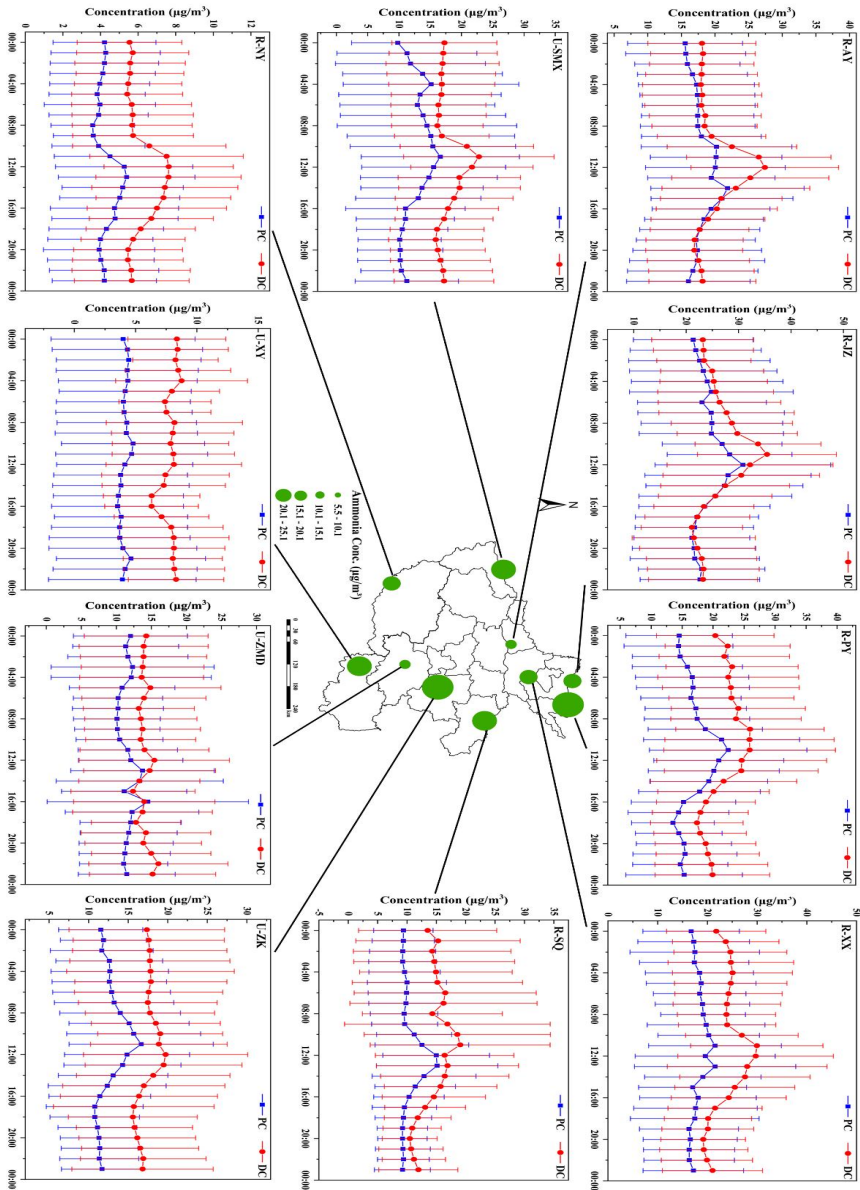
Figure 2. Daily variation of ammonia concentration at ten sites before (PC) and during (DC) the COVID-19 outbreak. The green dots represent the location of ten sites and their size represent the concentration of NH₃; the upper and lower whiskers represent the maximum and minimum values, respectively.

3.2 Gas-to-particle conversion of NH_3

213

214   Theoretically, the emissions of NH_3 from agricultural sources were not influenced

215 by the containment measures, and emissions from vehicles and industries would

216 decrease significantly in the DC. Consequently, the concentration of NH_3 should

217 decrease in the DC, which was opposite to the observed trends. The decreased NH_4^+ in

218 the DC suggests that the gas-particle partition of NH_3/ NH_4^+ may determine the

219 elevated NH_3 concentrations. Meteorological parameters, including RH and

220 temperature, play a crucial role in the gas-particle partitioning of NH_3 (Liu et al., 2023;

221 Xu et al., 2020). Therefore, the higher temperature and lower RH in the DC (Table S5)

222 favored the conversion of NH_4^+ to NH_3, resulting in a decrease in $\varepsilon(NH_4^+)$ ([NH

223 $_4^+$]/([NH_3] + [NH_4^+]) compared to those in the PC.

224   NH_3 primarily enters particles to neutralize acidic ions (Wang et al., 2020b; Xu et

225 al., 2020; Liu et al., 2017; Ye et al., 2011; Wells, 1998). Accordingly, the

226 concentrations of required ammonia (Required-NH_x) and excess ammonia (Excess-

227 NH_x) were calculated based on the acidic substances as follows (Wang et al., 2020b):

228
$$TNH_x = 17 \times (\frac{[NH_4^+]}{18} + \frac{[NH_3]}{17}) \quad (3.1)$$

229
$$Required\text{-}NH_x = 17 \times (\frac{[SO_4^{2-}]}{48} + \frac{[NO_3^-]}{63} + \frac{[Cl^-]}{35.5} + \frac{[HNO_3]}{64} + \frac{[HCl]}{36.5})$$
$$- 17 \times (\frac{[Na^+]}{23} + \frac{[K^+]}{39} + \frac{[Ca^{2+}]}{20} + \frac{[Mg^{2+}]}{12}) \quad (3.2)$$

230
$$Excess\text{-}NH_x = TNH_x - Required\text{-}NH_x \quad (3.3)$$

231 Where [W] represents the concentration of the substance ($\mu g/m^3$).

232   The significant linear fitting (R^2 is greater than 0.96, and the slope is close to 1)

233 in Figure S3 demonstrates that the anions and cations at each site are close to the

234 equilibrium state. Therefore, the organic acids in $PM_{2.5}$ had less effect on NH_3 and NH

235 $_4^+$, and were not considered in formula 3.2.

236   As shown in Figure 3 and Table S6, compared to those in the PC, the

237   concentration of Required-NH$_x$ in the DC significantly decreased (ranging from 37%

238   at site R-JZ to 58% at site R-PY), while the concentration of Excess-NH$_x$ increased

239   (ranging from 9% at site R-AY to 78% at site R-SQ). The reduction in the

240   concentrations of sulfate and nitrate (Figure S4) was responsible for the decrease in

241   the concentration of Required-NH$_x$. To sum up, in addition to meteorological

242   conditions, the substantial reduction in anthropogenic emissions of SO$_2$, NO$_x$, and

243   other pollutants in the DC has led to a decrease in acidic substances (e.g., sulfate and

244   nitrate) in particles, in turn, resulting in more gas-phase NH$_3$ concentration remaining

245   in the atmosphere.
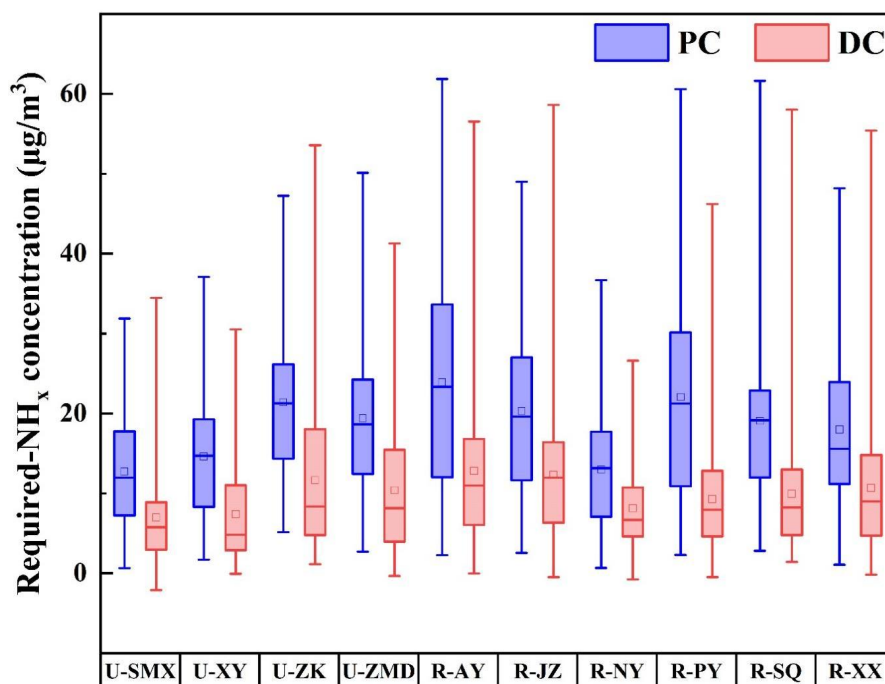
246

247   Figure 3. Box diagram of changes in Required-NH$_x$ at ten sites before (PC) and during (DC)

248   the COVID-19 outbreak. In each box, the top, middle, and bottom lines represent the 75, 50, and

249   25 percentiles of statistical data, respectively; the upper and lower whiskers represent the 90 and

250   10 percentiles of statistical data, respectively.

3.3 Particle pH before and during COVID-19

251

252 Previous studies have consistently reported that the concentration of Excess-NH_x

253 is the primary factor influencing the pH value of particles (Liu et al., 2023; Wang et

254 al., 2020b). Therefore, the U-ZK (4.3 μg/m³) and R-PY (7.5 μg/m³) with the largest

255 increase in Excess-NH_x concentration (Table S6) for urban and rural sites respectively

256 were selected to investigate the changes in particle pH value before and during the

257 pandemic. The pH values at U-ZK and R-PY were 4.7 and 4.8 in the PC, respectively,

258 which were close to the values in previous studies (Table S7). The higher pH values at

259 the rural site than those in the urban site can be attributed to the higher concentration

260 of Excess-NH_x in rural areas.

261 Note that Figure 4 suggests that the particle pH increased in the DC, with an

262 increase of 0.4 and 0.1 at U-ZK and R-PY, respectively. To explore the dominant

263 factors that determine the local particle pH level and result in the high pH during the

264 DC, sensitivity tests of pH to chemical species (i.e., TNH_x, TH_2SO_4, TNO_3, TCl, TNa,

265 K^+, Ca^{2+}, and Mg^{2+}) and meteorological parameters (i.e., T and RH) were performed.

266 A given range for a variable for U-ZK and R-PY two sites with corresponding average

267 values of other parameters was simulated to compare its effects on pH, the input data

268 was collected as shown in Figure 5 and Figure S5. The uncertainty of pH is shown in

269 Figure S6. Compared to PC, even though the decrease in TNH_x concentration and the

270 increase in temperature led to a decrease in pH values (0.09 at U-ZK and 0.08 at R-

271 PY site), this effect was outweighed by the decrease in TH_2SO_4 (0.07 and 0.8 at U-ZK

272 and R-PY site, respectively) and TNO_3 (0.05 and 0.4 at U-ZK and R-PY site,

273 respectively) concentrations as well as the increase in K^+ (0.03 at U-ZK and 0.2 at R-

274 PY site) and Mg^{2+} (0.01 at U-ZK and 0.04 at R-PY site) concentrations in the DC, and

275 resulting in an overall increase in pH values in the DC.

276
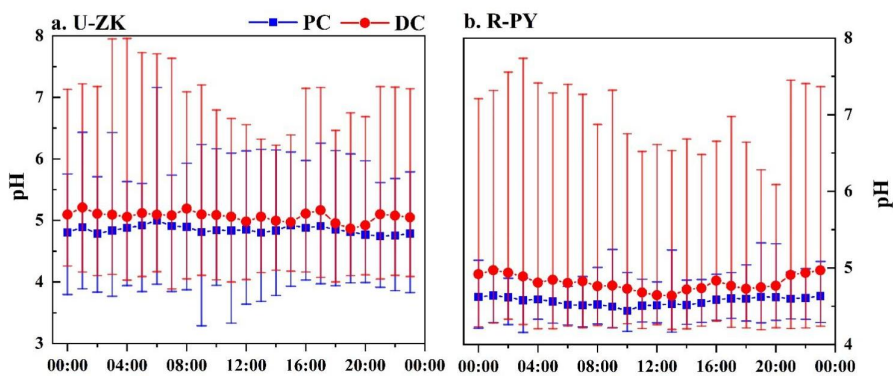
Figure 4. Daily variations of particle pH at a. U-ZK and b. R-PY sites before (PC) and during

(DC) the COVID-19 outbreak. The upper and lower whiskers represent the maximum and

minimum values, respectively.
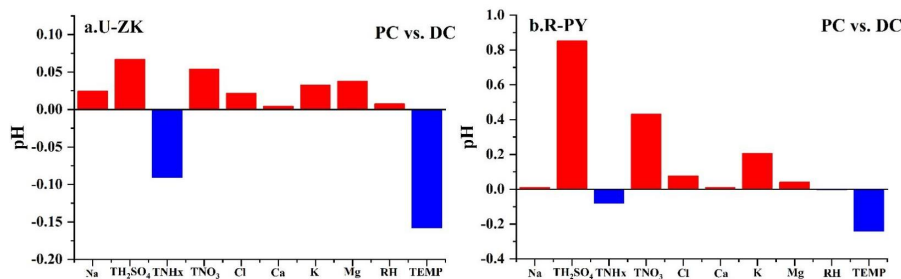
Figure 5. Comparison of pH sensitivity (Fig. S5) to each substance by changing paraments at a.

U-ZK and b. R-PY sites before (PC) and during (DC) the COVID-19 outbreak.

3.4 The influence of pH on HONO.

The observed HONO concentrations decreased by 18% and 54% at U-ZK (0.8

ppb) and R-PY (0.9 ppb) sites in the DC, respectively, compared to those (1.0 and 2.2

ppb) in the PC. Moreover, all the known HONO production sources rates including

P_{emi}, $P_{OH + NO}$, P_{ground}, $P_{ground+hv}$, $P_{aerosol}$, $P_{aerosol+hv}$, and $P_{nitrate}$ (Figure 6) show a

decreasing trend from PC to DC, with the mean reductions of 38% and 80% for U-ZK

and R-PY, respectively. At the U-ZK, $P_{ground+hv}$ decreased the most (84%), while at the

16

293 R-PY, $P_{nitrate}$ had the largest decrease about 85%, which is speculated to be related to

294 the decrease of NO_x and NO_3^- concentration in DC. Note that the reduction in the

295 overall known source and almost individual sources were greater than the reduction in

296 HONO concentrations (Figure 6 and 7), thus we hypothesized that there should be

297 other sources capable of promoting HONO production.
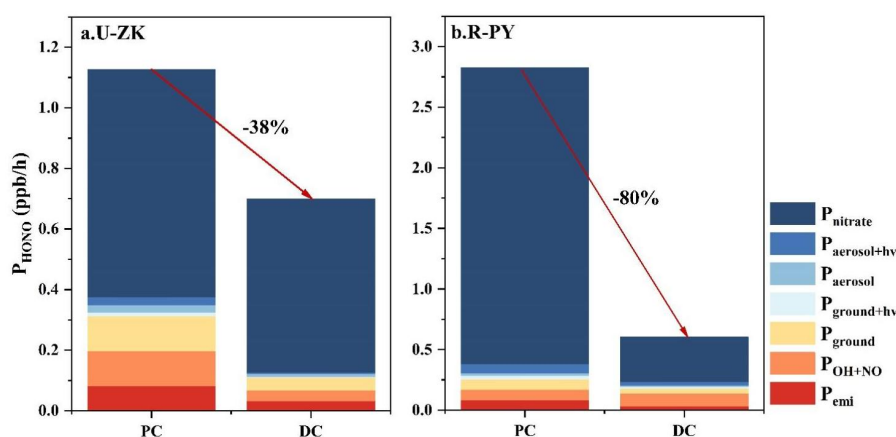
298

299 Figure 6. Comparison of HONO sources at a. U-ZK and b. R-PY sites before (PC) and during

300 (DC) the COVID-19 outbreak.

301

302 The relationship between HONO concentrations and other major influences at

303 the U-ZK and R-PY sites in the DC is displayed in Figure S7. HONO emissions were

304 affected by temperature to some extent(Liu et al., 2020c; Liu et al., 2020b), but there

305 was no significant positive correlation with temperature(Feng et al., 2022b), and

306 temperatures did not exceed a maximum of 10°C during this study period, suggesting

307 that soil emissions may not have been a major contributor to the PC HONOs during

308 this study period. In addition, the positive correlations between HONO with SO_2,

309 Excess-NH_x, SO_4^{2-}, and pH indicate that the R_1 reaction may also form an amount of

310 HONO and contribute to less reduction in the observed HONO concentrations.

311 Considering that R_1 mainly reacts in the liquid phase, the calculated reaction

312 rates of R_1 under the conditions of RH > 60% in the PC and DC periods are illustrated

313 in Figure 7. Despite the decrease in NO_2 and SO_2 concentrations in the DC, the

314   increase in particle pH, increasing HSO_3^- concentration in the aqueous phase,

315   promoted the R_1 reaction rates by 58% and 59% at U-ZK and R-PY (Figure 7),

316   respectively. Consequently, the enhanced R_1 reaction prevented a large decrease in

317   HONO (18% at U-ZK and 53% at R-PY) under the conditions of a significant

318   reduction in vehicle emissions and a decline of 66% and 69% in NO_2 concentrations

319   at U-ZK and R-PY, respectively.
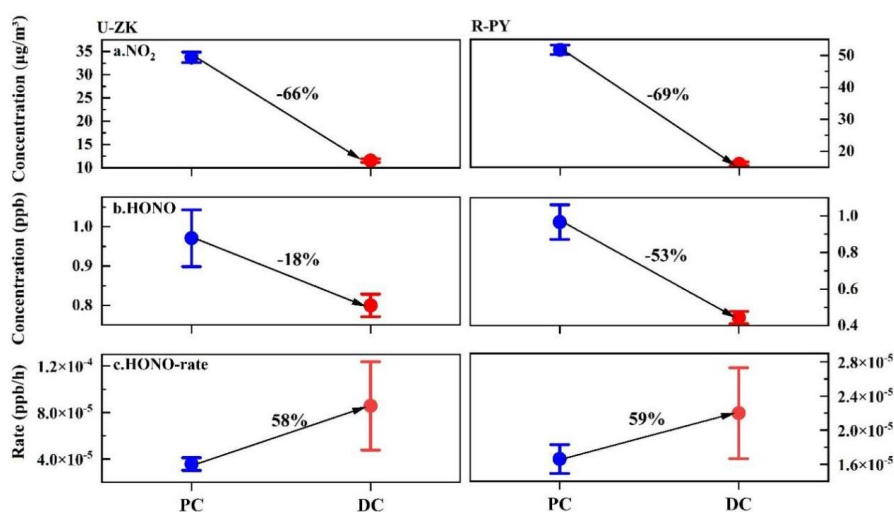
321   Figure 7. Decline ratios of a. NO_2, b. HONO concentration, and c. HONO production rate at U-

322   ZK and R-PY sites before (PC) and during (DC) the COVID-19 outbreak. The center point

323   represents the mean value, and the upper and lower whiskers represent the 95% confidence

324   interval of the mean.

3.5 Uncertainty

327   According to sensitivity tests of pH (Figure S5) and R_1 (Figure S8), pH

328   increases with the concentrations of cations (TNH_x, TNa, K^+, Ca^{2+}, and Mg^{2+}) and OC

329   increasing as well as anions (TH_2SO_4, TNO_3, and TCl) concentrations, Temp, and RH

330   decreasing. R_1 reaction rate increases with the concentrations of pH, AWC, NO_2, SO_2,

331   and Pressure (Pre), while increasing as well as T (K) decreasing. Therefore, two

332   extreme scenarios (i.e., the maximum and minimum rate scenarios) were evaluated to

333   estimate the uncertainty of AWC, pH, and R_1 HONO production rate based on the

334   measurement uncertainties at the U-ZK and R-PY sites. Figure S6 suggests that the

335   two extreme scenarios can be led to–10–7% and –71–125% uncertainties at the U-ZK

336   site and –10–7% and –78–123% uncertainties at the R-PY site for pH and R_1,

337   respectively.

338

4. Conclusions

340   Elevated NH_3 concentration was observed during the COVID-19 pandemic at

341   both urban and rural sites in China. In addition to the rise in temperature and decrease

342   in RH during the COVID-19 pandemic, which favored the conversion of NH_4^+ to NH_3,

343   the significant decrease in sulfate and nitrate concentrations led to the decline in

344   Required-NH_x and was beneficial to the particle-phase NH_4^+ portioning to gas-phase

345   NH_3. Furthermore, under the environmental conditions of increased NH_3

346   concentration and decreased acidic substance concentration, the pH values increased

347   by 0.4 and 0.1 at U-ZK and R-PY increased during the pandemic, respectively.

348   Consequently, the high pH values accelerated the formation rate of HONO through

349   the oxidation-reduction reaction of NO_2 with SO_2 (an increase of 58% at U-ZK and

350   59% at R-PY), partially compensating for the decrease in HONO concentration and

351   its sources caused by the decline in vehicle emissions and NO_2 concentration during

352   the COVID-19 pandemic.

353

5. Implications

355   HONO plays a crucial role as a precursor to OH radicals in the tropospheric

356 atmosphere (Xue, 2022). There have been significant observations of high HONO

357 concentrations in urban areas during the daytime, leading to a growing interest in

358 understanding its sources in atmospheric chemistry (Jiang et al., 2022; Xu et al.,

359 2019). The heterogeneous reaction mechanism of NO_2 on aerosol surfaces is currently

360 the focus of research on HONO sources, particularly in regions with elevated levels of

361 atmospheric particulate matter, where it could potentially become a major contributor

362 to HONO production (Zhang et al., 2022; Liao et al., 2021b). One of the pathways for

363 heterogeneous reactions on aerosol surfaces is the redox reaction of NO_2 with SO_2.

364 However, the significance of this reaction in HONO production in the real atmosphere

365 is often overlooked, as it relies on the high pH of aerosols (Ge et al., 2019). In recent

366 years, there has been increasing attention on the enhancing effect of NH_3 on the redox

367 reaction, with laboratory experiments demonstrating its ability to generate substantial

368 amounts of HONO (Ge et al., 2019). This study highlights the importance of this

369 reaction based on actual atmospheric observations. Furthermore, numerous studies

370 have indicated that if control over NH_3 emissions continues to relax while SO_2 and

371 NO_2 emissions decrease, the particle pH in future China is expected to rise steadily

372 (Xie et al., 2020; Song et al., 2019; Wang et al., 2020b). Consequently, the redox

373 reaction of NO_2 with SO_2 could become a significant source of HONO in China,

374 greatly amplifying the AOC. Therefore, it is crucial to coordinate the control of SO_2,

375 NO_x, and NH_3 emissions to avoid a rapid increase in the particle pH.

376

377 **Data availability:** All the data presented in this article can be accessed through

378 https://zenodo.org/records/10273539. (Zhang, 2023).

379   **Author contributions.** XZ Data Curation, Writing - Original Draft, Visualization.

380   LW, NW, SM and DZ Investigation, Visualization, Data Curation. DZ, HZ and MW

381   Investigation. SW Conceptualization, Data Curation, Supervision. RZ Data Curation,

382   Funding acquisition. All people involve in discussion of the results.

383

384   **Supplement.** The supplement related to this article is available online at: XXX.

385

386   **Competing interest.** The authors declare no competing financial interest.

387

References

Alicke, B.: OH formation by HONO photolysis during the BERLIOZ experiment, J. Geophy. Res.; 108, 8247, https://doi.org/10.1029/2001JD000579, 2003.

Atkinson, R., Baulch, D.L., Cox, R.A., Crowley, J.N., Hampson, R.F., Hynes, R.G., Jenkin, M.E., and Rossi, M. J., Troe, J.: Evaluated kinetic and photochemical data for atmospheric chemistry: volume I - gas phase reactions of O_x, HO_x, NO_x and SO_x species., Atmos. Chem. Phys., 4,1461 – 1738, https://doi.org/10.5194/acp-4-1461-2004, 2004.

Bougiatioti, A., Nikolaou, P., Stavroulas, I., Kouvarakis, G., Weber, R., Nenes, A., Kanakidou, M., and Mihalopoulos, N.: Particle water and pH in the eastern Mediterranean: source variability and implications for nutrient availability, Atmos. Chem. Phys., 16, 4579 – 4591, https://doi.org/10.5194/acp-16-4579-2016, 2016.

Chang, Y., Zou, Z., Zhang, Y., Deng, C., Hu, J., Shi, Z., Dore, A. J., and Collett, J. L., Jr.: Assessing contributions of agricultural and nonagricultural emissions to atmospheric ammonia in a Chinese megacity. Environ. Sci. Technol. 53, 1822 – 1833., https://doi.org/10.1021/acs.est.8b05984, 2019.

Chen, X., Walker, J. T., and Geron, C.: Chromatography related performance of the monitor for aerosols and gases in ambient air (MARGA): laboratory and field-based evaluation. Atmos. Meas. Tech. 10, 3893 – 3908. https://doi.org/10.5194/amt-10-3893-2017, 2017.

Cheng, Y., Zheng, G., Wei, C., Mu, Q., Zheng, B., Wang, Z., Gao, M., Z., Q., He, K., Carmichael, G., Pöschl, U., and Su, and H.: Reactive nitrogen chemistry in aerosol water as a source of sulfate during haze events in China, Sci. Adv. 2, e1601530., https://doi.org/10.1126/sciadv.1601530, 2019.

Ding, J., Zhao, P., Su, J., Dong, Q., Du, X., and Zhang, Y.: Aerosol pH and its driving factors in Beijing, Atmos. Chem. Phys. 19, 7939 – 7954., https://doi.org/10.5194/acp-19-7939-2019, 2019.

420   Ellis, R. A., Murphy, J. G., Markovic, M. Z., VandenBoer, T. C., Makar, P. A., Brook,
421   J., and Mihele, C.: The influence of gas-particle partitioning and surface-
422   atmosphere exchange on ammonia during BAQS-Met, Atmos. Chem. Phys. 11,
423   133 – 145., https://doi.org/10.5194/acp-11-133-2011, 2011.

424   Feng, S., Xu, W., Cheng, M., Ma, Y., Wu, L., Kang, J., Wang, K., Tang, A., Collett, J.
425   L., Fang, Y., Goulding, K., Liu, X., and Zhang, F.: Overlooked nonagricultural
426   and wintertime agricultural NH_3 emissions in Quzhou county, north China plain:
427   evidence from ^{15}N-Stable Isotopes. Environ. Sci. Technol. Lett. 9, 127 – 133,
428   https://doi.org/10.1021/acs.estlett.1c00935, 2022a.

429   Feng, T., Zhao, S., Liu, L., Long, X., Gao, C., and Wu, N.: Nitrous acid emission from
430   soil bacteria and related environmental effect over the North China Plain,
431   Chemos., 287, https://doi.org/10.1016/j.chemosphere.2021.132034, 2022b.

432   Fountoukis, C., Nenes, A.: ISORROPIA II: a computationally efficient
433   thermodynamic equilibrium model for K^+-Ca^{2+}-Mg^{2+}-NH_4^+-Na^+-SO_4^{2-}-NO^{3-}-Cl^--
434   H_2O aerosols. Atmos. Chem. Phys. 7, 4639 – 4659, https://doi.org/10.5194/acp-
435   7-4639-2007, 2007.

436   Ge, S., Wang, G., Zhang, S., Li, D., and Zhang, H.: Abundant NH_3 in China enhances
437   atmospheric HONO production by promoting the heterogeneous reaction of SO_2
438   with NO_2. Environ. Sci. Technol. 53, 14339 – 14347,
439   https://doi.org/10.1021/acs.est.9b04196, 2019.

440   Gong, L., Lewicki, R., Griffin, R. J., Flynn, J. H., Lefer, B. L., and Tittel, F. K.:
441   Atmospheric ammonia measurements in Houston, TX using an external-cavity
442   quantum cascade laser-based sensor, Atmos. Chem. and Phys. 11, 9721 – 9733,
443   https://doi.org/10.5194/acp-11-9721-2011, 2011.

444   Gu, M., Pan, Y., Walters, W. W., Sun, Q., Song, L., Wang, Y., Xue, Y., and Fang, Y.:
445   ehicular emissions enhanced ammonia concentrations in winter mornings:
446   insights from diurnal nitrogen isotopic signatures. Environ. Sci. Technol. 56,
447   1578 – 1585, https://doi.org/10.1021/acs.est.1c05884, 2022.

448   Han, S., Hong, J., Luo, Q., Xu, H., Tan, H., Wang, Q., Tao, J., Zhou, Y., Peng, L., He,
449   Y., Shi, J., Ma, N., Cheng, Y., and Su, H.: Hygroscopicity of organic compounds

450   as a function of organic functionality, water solubility, molecular weight, and
451   oxidation level, Atmos. Chem. Phys., 22, 3985 – 4004,
452   https://doi.org/10.5194/acp-22-3985-2022, 2022.

453 Huang, X., Ding, A., Gao, J., Zheng, B., Zhou, D., Qi, X., Tang, R., Wang, J., Ren, C.,
454   Nie, W., Chi, X., Xu, Z., Chen, L., Li, Y., Che, F., Pang, N., Wang, H., Tong, D.,
455   Qin, W., Cheng, W., Liu, W., Fu, Q., Liu, B., Chai, F., Davis, S. J., Zhang, Q.,
456   and He, K.: Enhanced secondary pollution offset reduction of primary emissions
457   during COVID-19 lockdown in China, Natl Sci Rev, 8, nwaa137,
458   https://doi.org/10.1093/nsr/nwaa137, 2021a.

459 Huang, X., Zhang, J., Zhang, W., Tang, G., and Wang, Y.: Atmospheric ammonia and
460   its effect on $PM_{2.5}$ pollution in urban Chengdu, Sichuan Basin, China. Environ.
461   Pollut. 291, 118 – 195. https://doi.org/10.1016/j.envpol.2021.118195, 2021b.

462 Jiang, Y., Xue, L., Shen, H., Dong, C., Xiao, Z., and Wang, W.: Dominant processes
463   of HONO derived from multiple field observations in contrasting environments.
464   Environ. Sci. Technol. Lett. 9, 258 – 264,
465   https://doi.org/10.1021/acs.estlett.2c00004, 2022.

466 Kramer, L. J., Crilley, L. R., Adams, T. J., Ball, S. M., Pope, F. D., and Bloss, W. J.:
467   Nitrous acid (HONO) emissions under real-world driving conditions from
468   vehicles in a UK road tunnel, Atmos. Chem. and Phys. 20, 5231 – 5248,
469   https://doi.org/10.5194/acp-20-5231-2020, 2020.

470 Li, J., An, X., Cui, M., Sun, Z., Wang, C., and Li, Y.: Simulation study on regional
471   atmospheric oxidation capacity and precursor sensitivity, Atmos. Environ. 263,
472   118657, https://doi.org/10.1016/j.atmosenv.2021.118657, 2021a.

473 Li, S., Song, W., Zhan, H., Zhang, Y., Zhang, X., Li, W., Tong, S., Pei, C., Wang, Y.,
474   Chen, Y., Huang, Z., Zhang, R., Zhu, M., Fang, H., Wu, Z., Wang, J., Luo, S., Fu,
475   X., Xiao, S., Huang, X., Zeng, J., Zhang, H., Chen, D., Gligorovski, S., Ge, M.,
476   George, C., and Wang, X.: Contribution of vehicle emission and NO_2 surface
477   conversion to nitrous acid (HONO) in urban environments: implications from
478   tests in a tunnel. Environ. Sci. Technol., 55, 15616 – 15624,
479   https://doi.org/10.1021/acs.est.1c00405, 2021b.

480   Li, Y., Han, Z., Song, Y., Li, J., Sun, Y., and Wang, T.: Impacts of the COVID-19

481   lockdown on atmospheric oxidizing capacity and secondary aerosol formation

482   over the Beijing-Tianjin-Hebei region in Winter-Spring 2020, Atmos. Environ.

483   295, 119540, https://doi.org/10.1016/j.atmosenv.2022.119540, 2023.

484   Liao, S., Zhang, J., Yu, F., Zhu, M., Liu, J., Ou, J., Dong, H., Sha, Q., Zhong, Z., Xie,

485   Y., Luo, H., Zhang, L., and Zheng, J.: High gaseous nitrous acid (HONO)

486   emissions from light-duty diesel vehicles. Environ. Sci. Technol. 55, 200 – 208,

487   https://doi.org/10.1021/acs.est.0c05599, 2021.

488   Liu, J., Deng, H., Lakey, P. S. J., Jiang, H., Mekic, M., Wang, X., Shiraiwa, M., and

489   Gligorovski, S.: Unexpectedly high indoor HONO concentrations associated

490   with photochemical NO_2 transformation on glass windows. Environ. Sci.

491   Technol. 54, 15680 – 15688, https://doi.org/10.1021/acs.est.0c05624, 2020a.

492   Liu, L., Zhang, J., Du, R., Teng, X., Hu, R., Yuan, Q., Tang, S., Ren, C., Huang, X.,

493   Xu, L., Zhang, Y., Zhang, X., Song, C., Liu, B., Lu, G., Shi, Z., and Li, W.:

494   Chemistry of atmospheric fine particles during the COVID-19 pandemic in a

495   megacity of eastern China. Geophys. Res. Lett. 48, 2020GL091611,

496   https://doi.org/10.1029/2020GL091611, 2021.

497   Liu, M., Song, Y., Zhou, T., Xu, Z., Yan, C., Zheng, M., Wu, Z., Hu, M., Wu, Y., and

498   Zhu, T.: Fine particle pH during severe haze episodes in northern China.

499   Geophys. Res. Lett. 44, 5213 – 5221, https://doi.org/10.1002/2017gl073210,

500   2017.

501   Liu, P., Chen, H., Song, Y., Xue, C., Ye, C., Zhao, X., Zhang, C., Liu, J., and Mu, Y.:

502   Atmospheric ammonia in the rural North China Plain during wintertime:

503   variations, sources, and implications for HONO heterogeneous formation. Sci.

504   Total. Environ. 861, 160768, https://doi.org/10.1016/j.scitotenv.2022.160768,

505   2023.

506   Liu, Y., Ni, S., Jiang, T., Xing, S., Zhang, Y., Bao, X., Feng, Z., Fan, X., Zhang, L.,

507   and Feng, H.: Influence of Chinese New Year overlapping COVID-19 lockdown

508   on HONO sources in Shijiazhuang, Sci. Total Environ., 745, 141025,

509   https://doi.org/10.1016/j.scitotenv.2020.141025, 2020b.

510   Liu, Y., Zhang, Y., Lian, C., Yan, C., Feng, Z., Zheng, F., Fan, X., Chen, Y., Wang, W.,

511   Chu, B., Wang, Y., Cai, J., Du, W., Daellenbach, K. R., Kangasluoma, J., Bianchi,

512   F., Kujansuu, J., Petäjä, T., Wang, X., Hu, B., Wang, Y., Ge, M., He, H., and

513   Kulmala, M.: The promotion effect of nitrous acid on aerosol formation in

514   wintertime in Beijing: the possible contribution of traffic-related emissions,

515   Atmos. Chem. Phys, 20, 13023 – 13040, https://doi.org/10.5194/acp-20-13023-

516   2020, 2020c.

517   Liu, Z., Wang, Y., Costabile, F., Amoroso, A., Zhao, C., Huey, L. G., Stickel, R., Liao,

518   J., and Zhu, T.: Evidence of aerosols as a media for rapid daytime HONO

519   production over China, Environ. Sci. Technol., 48, 13023 – 13040,

520   https://doi.org/10.1021/es504163z, 2014.

521   Luo, L., Bai, X., Lv, Y., Liu, S., Guo, Z., Liu, W., Hao, Y., Sun, Y., Hao, J., Zhang, K.,

522   Zhao, H., Lin, S., Zhao, S., Xiao, Y., Yang, J., and Tian, H.: Exploring the driving

523   factors of haze events in Beijing during Chinese New Year holidays in 2020 and

524   2021 under the influence of COVID-19 pandemic, Sci. Total Environ., 859,

525   160172, https://doi.org/10.1016/j.scitotenv.2022.160172, 2023.

526   Ma, S.: High-resolution assessment of ammonia emissions in China: Inventories,

527   driving   forces   and   mitigation,   Atmos.   Environ.,   229,

528   https://doi.org/10.1016/j.atmosenv.2020.117458, 2020.

529   McFall, A. S., Edwards, K. C., and Anastasio, C.: Nitrate Photochemistry at the Air-

530   Ice Interface and in Other Ice Reservoirs, Environ. Sci. Technol., 52, 5710 –

531   5717, https://doi.org/10.1021/acs.est.8b00095, 2018.

532   Meng, Z., Xu, X., Lin, W., Ge, B., Xie, Y., Song, B., Jia, S., Zhang, R., Peng, W.,

533   Wang, Y., Cheng, H., Yang, W., and Zhao, H.: Role of ambient ammonia in

534   particulate ammonium formation at a rural site in the North China Plain, Atmos.

535   Chem. Phys., 18, 167 – 184, https://doi.org/10.5194/acp-18-167-2018, 2018.

536   Meusel, H., Tamm, A., Kuhn, U., Wu, D., Leifke, A. L., Fiedler, S., Ruckteschler, N.,

537   Yordanova, P., Lang-Yona, N., Pöhlker, M., Lelieveld, J., Hoffmann, T., Pöschl,

538   U., Su, H., Weber, B., and Cheng, Y.: Emission of nitrous acid from soil and

539   biological soil crusts represents an important source of HONO in the remote

540   atmosphere in Cyprus, Atmos. Chem. Phys., 18, 799 – 813,
541   https://doi.org/10.5194/acp-18-799-2018, 2018.

542   Oswald, R., Behrendt, T., Ermel, M., Wu, D., Su, H., Cheng, Y., Breuninger, C.,
543   Moravek, A., Mougin, E., Delon, C., Loubet, B., Pommerening-Roser, A., Sorgel,
544   M., Poschl, U., and Hoffmann, T., Andreae, M.O., Meixner, F.X., Trebs, I.:
545   HONO emissions from soil bacteria as a major source of atmospheric reactive
546   nitrogen., Science. 341, 1233 – 1235,
547   https://www.science.org/doi/10.1126/science.1242266, 2013.

548   Pagsberg, P., Bjergbakke, E., Ratajczak, E., Sillesen, A.: Kinetics of the gas phase
549   reaction OH + NO (+M)-> HONO (+M) and the determination of the UV
550   absorption cross sections of HONO., Chem. Phys. Lett. 272, 383 – 390,
551   https://doi.org/10.1016/s0009-2614(97)00576-9, 1997.

552   Romer, P. S., Wooldridge, P. J., Crounse, J. D., Kim, M. J., Wennberg, P. O., Dibb, J.
553   E., Scheuer, E., Blake, D. R., Meinardi, S., Brosius, A. L., Thames, A. B., Miller,
554   D. O., Brune, W. H., Hall, S. R., Ryerson, T. B., and Cohen, R. C.: Constraints on
555   aerosol nitrate photolysis as a potential source of HONO and NOx. Environ. Sci.
556   Technol. 52, 13738 – 13746, https://doi.org/10.1021/acs.est.8b03861, 2018.

557   Scharko, N. K., Berke, A. E., and Raff, J. D.: Release of nitrous acid and nitrogen
558   dioxide from nitrate photolysis in acidic aqueous solutions, Environ. Sci.
559   Technol., 48, 11991 – 12001, https://doi.org/10.1021/es503088x, 2014.

560   Shi, Q., Tao, Y., Krechmer, J. E., Heald, C. L., Murphy, J. G., Kroll, J. H., and Ye, Q.:
561   Laboratory Investigation of Renoxification from the Photolysis of Inorganic
562   Particulate Nitrate, Environ. Sci. Technol., 55, 854 – 861,
563   https://doi.org/10.1021/acs.est.0c06049, 2021.

564   Song, S., Gao, M., Xu, W., Shao, J., Shi, G., Wang, S., Wang, Y., Sun, Y., and
565   McElroy, M. B.: Fine-particle pH for Beijing winter haze as inferred from
566   different thermodynamic equilibrium models, Atmos. Chem. Phys., 18, 7423 –
567   7438, https://doi.org/10.5194/acp-18-7423-2018, 2018.

568   Song, S., Nenes, A., Gao, M., Zhang, Y., Liu, P., Shao, J., Ye, D., Xu, W., Lei, L., Sun,
569   Y., Liu, B., Wang, S., and McElroy, M. B.: Thermodynamic modeling suggests

570   declines in water uptake and acidity of inorganic aerosols in Beijing winter haze

571   events during 2014/2015–2018/2019. Environ. Sci. Technol. Lett. 6, 752 – 760,

572   https://doi.org/10.1021/acs.estlett.9b00621, 2019.

573   Spataro, F., and Ianniello, A.: Sources of atmospheric nitrous acid: state of the science,

574   current research needs, and future prospects, J. Air. Waste. Manag. Assoc., 64,

575   1232 – 1250, https://doi.org/10.1080/10962247.2014.952846, 2014.

576   Stieger, B., Spindler, G., van Pinxteren, D., Grüner, A., Wallasch, M., and Herrmann,

577   H.: Development of an online-coupled MARGA upgrade for the 2 h interval

578   quantification of low-molecular-weight organic acids in the gas and particle

579   phases, Atmos. Meas. Tech. 12, 281 – 298, https://doi.org/10.5194/amt-12-281-

580   2019, 2019.

581   Su, H., Cheng, Y., Oswald, R., Behrendt, T., Trebs, I., Meixner, F.X., Andreae, M.O.,

582   Cheng, P., and Zhang, Y., Poschl, U.: Soil nitrite as a source of atmospheric

583   HONO   and   OH   radi   cals.,   Science.   333,   1616   –   1618,

584   https://doi.org/10.1126/science.1207687, 2011.

585   Tian, H., Liu, Y., Li, Y., Wu, C.-H., Chen, B., Kraemer, M. U. G.: An investigation of

586   transmission control measures during the first 50 days of the COVID-19

587   epidemic   in   China.,   Science,   368:   638   –   642,

588   https://doi.org/10.1126/science.abb6105, 2020.

589   Twigg, M. M., Berkhout, A. J. C., Cowan, N., Crunaire, S., Dammers, E., Ebert, V.,

590   Gaudion, V., Haaima, M., Häni, C., John, L., Jones, M. R., Kamps, B.,

591   Kentisbeer, J., Kupper, T., Leeson, S. R., Leuenberger, D., Lüttschwager, N. O.

592   B., Makkonen, U., Martin, N. A., Missler, D., Mounsor, D., Neftel, A., Nelson,

593   C., Nemitz, E., Oudwater, R., Pascale, C., Petit, J.-E., Pogany, A., Redon, N.,

594   Sintermann, J., Stephens, A., Sutton, M. A., Tang, Y. S., Zijlmans, R., Braban, C.

595   F., and Niederhauser, B.: Intercomparison of in situ measurements of ambient

596   NH3: instrument performance and application under field conditions, Atmos.

597   Meas. Tech. 15, 6755 – 6787, https://doi.org/10.5194/amt-15-6755-2022, 2022.

598   Wang, C., Yin, S., Bai, L., Zhang, X., Gu, X., Zhang, H., Lu, Q., and Zhang, R.: High-

599   resolution ammonia emission inventories with comprehensive analysis and

600   evaluation in Henan, China, 2006–2016, Atmos. Environ. 193, 11 – 23,
601   https://doi.org/10.1016/j.atmosenv.2018.08.063, 2018.

602   Wang, P., Chen, K., Zhu, S., Wang, P., and Zhang, H.: Severe air pollution events not
603   avoided by reduced anthropogenic activities during COVID-19 outbreak, Resour.
604   Conserv. Recycl., 158, 104814, https://doi.org/10.1016/j.resconrec.2020.104814,
605   2020a.

606   Wang, S., Wang, L., Li, Y., Wang, C., Wang, W., Yin, S., and Zhang, R.: Effect of
607   ammonia on fine-particle pH in agricultural regions of China: comparison
608   between urban and rural sites, Atmos. Chem. Phys., 20, 2719 – 2734,
609   https://doi.org/10.5194/acp-20-2719-2020, 2020b.

610   Wang, S., Wang, L., Fan, X., Wang, N., Ma, S., and Zhang, R.: Formation pathway of
611   secondary inorganic aerosol and its influencing factors in Northern China:
612   Comparison between urban and rural sites, Sci. Total Environ., 840,
613   https://doi.org/10.1016/j.scitotenv.2022.156404, 2022.

614   Wang, S., Fan, X., Xu, Y., Zhang, R., and Ren, B.: Insight into the non-linear
615   responses of particulate sulfate to reduced SO_2 concentration: A perspective from
616   the aqueous-phase reactions in a megacity in Northern China, Atmos. Res., 290,
617   https://doi.org/10.1016/j.atmosres.2023.106796, 2023a.

618   Wang, W., Wang, S., Xu, J., Zhou, R., Shi, C., and Zhou, B.: Gas-phase ammonia and
619       $PM_{2.5}$ ammonium in a busy traffic area of Nanjing, China, Environ. Sci. Pollut.
620   Res. Int., 23, 1691 – 1702, https://doi.org/10.1007/s11356-015-5397-3, 2016.

621   Wang, Y., Zhu, S., Ma, J., Shen, J., Wang, P., Wang, P., and Zhang, H.: Enhanced
622   atmospheric oxidation capacity and associated ozone increases during COVID-
623   19 lockdown in the Yangtze River Delta, Sci. Total Environ., 768, 144796,
624   https://doi.org/10.1016/j.scitotenv.2020.144796, 2021.

625   Wang, Y., Jin, X., Liu, Z., Wang, G., Tang, G., Lu, K., Hu, B., Wang, S., Li, G., An, X.,
626   Wang, C., Hu, Q., He, L., Zhang, F., and Zhang, Y.: Progress in quantitative
627   research on the relationship between atmospheric oxidation and air quality, J.
628   Environ. Sci., 123, 350 – 366, https://doi.org/10.1016/j.jes.2022.06.029, 2023b.

629   Wells, M., Choularton, T. W., and Bower, K. N.: A modelling study of the interaction

630 of ammonia with cloud., Atmos. Environ., 32, 359 – 363,
631 https://doi.org/10.1016/s1352-2310(97)00199-4, 1998.

632 Wentworth, G. R., Murphy, J. G., Benedict, K. B., Bangs, E. J., and Collett Jr, J. L.:
633 The role of dew as a night-time reservoir and morning source for atmospheric
634 ammonia, Atmos. Chem. Phys. 16, 7435 – 7449, https://doi.org/10.5194/acp-16-
635 7435-2016, 2016.

636 Wu, C., Lv, S., Wang, F., Liu, X., Li, J., Liu, L., Zhang, S., Du, W., Liu, S., Zhang, F.,
637 Li, J., Meng, J., and Wang, G.: Ammonia in urban atmosphere can be
638 substantially reduced by vehicle emission control: A case study in Shanghai,
639 China, J. Environ. Sci., 126, 754 – 760, https://doi.org/10.1016/j.jes.2022.04.043,
640 2023.

641 Xie, Y., Wang, G., Wang, X., Chen, J., Chen, Y., Tang, G., Wang, L., Ge, S., Xue, G.,
642 Wang, Y., and Gao, J.: Nitrate-dominated PM2.5 and elevation of particle pH
643 observed in urban Beijing during the winter of 2017. Atmos. Chem. Phys. 20,
644 5019 – 5033, https://doi.org/10.5194/acp-20-5019-2020, 2020.

645 Xu, J., Chen, J., Zhao, N., Wang, G., Yu, G., Li, H., Huo, J., Lin, Y., Fu, Q., Guo, H.,
646 Deng, C., Lee, S.-H., Chen, J., and Huang, K.: Importance of gas-particle
647 partitioning of ammonia in haze formation in the rural agricultural environment,
648 Atmos. Chem. Phys. 20, 7259 – 7269, https://doi.org/10.5194/acp-20-7259-2020,
649 2020.

650 Xu, W., Kuang, Y., Zhao, C., Tao, J., Zhao, G., Bian, Y., Yang, W., Yu, Y., Shen, C.,
651 Liang, L., Zhang, G., Lin, W., and Xu, X.: NH3-promoted hydrolysis of NO2
652 induces explosive growth in HONO, Atmos. Chem. and Phys. 19, 10557 – 10570,
653 https://doi.org/10.5194/acp-19-10557-2019, 2019.

654 Xu, W., Zhao, Y., Wen, Z., Chang, Y., Pan, Y., Sun, Y., Ma, X., Sha, Z., Li, Z., Kang,
655 J., Liu, L., Tang, A., Wang, K., Zhang, Y., Guo, Y., Zhang, L., Sheng, L., Zhang,
656 X., Gu, B., Song, Y., Van Damme, M., Clarisse, L., Coheur, P. F., Collett, J. L.,
657 Jr., Goulding, K., Zhang, F., He, K., and Liu, X.: Increasing importance of
658 ammonia emission abatement in PM$_{2.5}$ pollution control. Sci. Bull. 67, 1745 –
659 1749, https://doi.org/10.1016/j.scib.2022.07.021, 2022.

660 Xue, C.: Substantially growing interest in the chemistry of nitrous acid (HONO) in
661   China: current achievements, problems, and future directions. Environ. Sci.
662   Technol. 56, 7375 – 7377. https://doi.org/10.1021/acs.est.2c02237, 2022.

663 Ye, C., Zhang, N., Gao, H., and Zhou, X.: Photolysis of particulate nitrate as a source
664   of HONO and NO_x. Environ. Sci. Technol. 51, 6849 – 6856,
665   https://doi.org/10.1021/acs.est.7b00387, 2017.

666 Ye, X., Ma, Z., Zhang, J., Du, H., Chen, J., Chen, H., Yang, X., Gao, W., and Geng, F.:
667   Important role of ammonia on haze formation in Shanghai, Environ. Res. Lett. 6,
668   024019, https://doi.org/10.1088/1748-9326/6/2/024019, 2011.

669 Zhang, W., Tong, S., Jia, C., Wang, L., Liu, B., Tang, G., Ji, D., Hu, B., Liu, Z., Li, W.,
670   Wang, Z., Liu, Y., Wang, Y., and Ge, M.: Different HONO sources for three
671   layers at the urban area of Beijing. Environ. Sci. Technol. 54, 12870 – 12880,
672   https://doi.org/10.1021/acs.est.0c02146, 2020a.

673 Zhang, W., Tong, S., Jia, C., Ge, M., Ji, D., Zhang, C., Liu, P., Zhao, X., Mu, Y., Hu,
674   B., Wang, L., Tang, G., Li, X., Li, W., and Wang, Z.: Effect of different
675   combustion processes on atmospheric nitrous acid formation mechanisms: a
676   winter comparative observation in urban, suburban and rural areas of the North
677   China   Plain.   Environ.   Sci.   Technol.   56,   4828   –   4837,
678   https://doi.org/10.1021/acs.est.1c07784, 2022.

679 Zhang, X., Tong, S., Jia, C., Zhang W., Wang Z., Tang G., Hu B., Liu Z., Wang L.,
680   Zhao P., Pan Y., Ge M.: Elucidating HONO formation mechanism and its
681   essential contribution to OH during haze events. Npj. Clim. Atmos. Sci.; 6, 55,
682   https://doi.org/10.1038/s41612-023-00371-w, 2023.

683 Zhang, Y., Liu, X., Fang, Y., Liu, D., Tang, A., and Collett, J. L.: Atmospheric
684   ammonia in Beijing during the COVID-19 outbreak: concentrations, sources, and
685   implications.   Environ.   Sci.   Technol.   Lett.   8,   32   –   38,
686   https://doi.org/10.1021/acs.estlett.0c00756, 2020b.

687 Zheng, H., Kong, S., Chen, N., Yan, Y., Liu, D., Zhu, B., Xu, K., Cao, W., Ding, Q.,
688   Lan, B., Zhang, Z., Zheng, M., Fan, Z., Cheng, Y., Zheng, S., Yao, L., Bai, Y.,
689   Zhao, T., and Qi, S.: Significant changes in the chemical compositions and

690   sources of PM$_{2.5}$ in Wuhan since the city lockdown as COVID-19. Sci. Total

691   Environ. 739: 140000, https://doi.org/10.1016/j.scitotenv.2020.140000, 2020.

692